Proteomic Characterization of Engineered Nanomateria, Protein Interactions in Relation to Surface Reactivity.

5 AUTHORS, INCLUDING:

Jukka Sund
Finnish Institute of Occupational Health
6 PUBLICATIONS **255** CITATIONS

SEE PROFILE

Minnamari Vippola
Tampere University of Technology
96 PUBLICATIONS **1,400** CITATIONS

SEE PROFILE

Kai Savolainen
Finnish Institute of Occupational Health
253 PUBLICATIONS **4,137** CITATIONS

SEE PROFILE

Anne Puustinen
Finnish Institute of Occupational Health
62 PUBLICATIONS **3,374** CITATIONS

SEE PROFILE

Proteomic Characterization of Engineered Nanomaterial–Protein Interactions in Relation to Surface Reactivity

Jukka Sund,[†] Harri Alenius,[†] Minnamari Vippola,[‡,⊥] Kai Savolainen,[§] and Anne Puustinen[†,*]

[†]Unit for Immunotoxicology, Health and Work Ability, [‡]Aerosols, Metals and Dusts, Work Environment Development, and [§]New Technologies and Risks, Work Environment Development, Finnish Institute of Occupational Health, Helsinki, Finland, and [⊥]Department of Materials Science, Tampere University of Technology, Tampere, Finland.

The numerous possibilities of engineered nanomaterials (ENMs) have led to fast growth of industries utilizing ENMs. This creates a need to determine physicochemical properties of each material and to evaluate the biological response due to exposure to the developed ENMs. Engineered nanomaterials have at least one dimension less than 100 nm. Their small size enables nanoparticles to have distinct physicochemical properties, which have been applied to electronics, cosmetics, and clinical applications.[1−3] A number of studies relating to ENM toxicity have already been published, where ENMs have been shown to cause, for example, inflammation, DNA damage, and cancer.[4−6] However, much less is known about the mechanisms of interactions between biomolecules and nanoparticles.

ENMs, when entering the organism, become coated with proteins of biofluids, which leads to a protein corona surrounding the nanoparticle. The nature of this coating determines the final biological identity of the particle.[7] Physico-chemical properties that define the fate of the particle inside a body are size, chemical composition, shape, and surface reactivity. The main determinants of surface reactivity are surface charge (zeta potential) and surface modifications, which affect the chemical properties and solubility of the particle.[8−10] Surface reactivity can also have an effect on particle toxicity, as it specifies the composition of the protein corona and modulates the reactivity toward cells and tissues.[11] Biophysical properties of each protein are also unique due to the primary amino acid sequence and

ABSTRACT Adsorption of proteins onto an engineered nanoparticle surface happens immediately after particles come in contact with a biological fluid. However, at the moment very little is known about the mechanisms of interactions between biomolecules and nanomaterials. In this study, eleven thoroughly characterized materials were first investigated *in vitro* for their ability to enter human lung epithelial cells and human monocyte-derived macrophages. All tested materials were taken up by primary macrophages and epithelial cells. Some of the engineered nanomaterials (ENM) were found in the cytoplasm. Large quantitative and qualitative variation in the binding efficiencies to cellular proteins was observed between different tested nanoparticles. Pulmonary surfactant components significantly reduced the overall protein adsorption on the surface of ENMs. Fibrinogen chains were attached to all materials after exposure to plasma proteins. Common ENM-bound cytoplasmic protein identifications were peroxiredoxin 1, annexin A2, and several ribosomal and cytoskeletal proteins. The underlying mechanism of the ENM-plasma protein interaction may diverge from that of cell lysate proteins, as the binding efficiency to cell lysate proteins appears to depend on the characteristics of the ENM surface, whereas the adsorbed plasma proteins are involved in particle phagocytosis and seem to cover ENMs independently of the their surface properties. Identification of the composition of the nanomaterial–protein complex is crucial for understanding of the uptake mechanisms, biodistribution, and clearance of ENMs, knowledge which is required for safety evaluation and biomedical applications of these materials.

post-translational modifications, (*e.g.*, glycosylation and phosphorylation). Phosphopeptide enrichment using titanium dioxide as affinity column material is one example of the applied interactions between metal oxides and proteins.[12]

The growing interest in nanotechnologies means increased exposure to ENMs. Contamination of the human body with ENM can happen through inhalation as well as through ingestion. Larger particles usually get stuck on the mucus-layer of the upper airways, whereas most of the nanosized materials are able to reach the alveoli because of their smaller size.[13] The deeper compartments of the lung are lined by a pulmonary surfactant layer, which is the initial contact surface for

ENMs after deposition in the alveolar region. It has been shown that nanomaterials can interact with protein and phospholipid components of the surfactant and that they can disturb surfactant function as a regulator of the surface tension at the air−liquid interface of the lower airways.[14,15] After penetrating the surfactant film ENMs can be taken up by various alveolar cell types including macrophages, epithelial cells, and dendritic cells.[16,17]

To study interactions between biological systems and ENMs *in vitro*, several metal oxide ENMs, two types of carbon nanotubes (CNTs), and fine-sized particles were tested for their cellular uptake by primary macrophages and alveolar epithelial cells. Capability of ENMs to adsorb proteins from plasma and cell lysate was also investigated, as well as the influence of surfactant components on these interactions. To further characterize the nature of protein binding to nanoparticles, isoelectric point values of the ENM bound proteins were compared after protein identification by tandem mass spectrometry, and the effect of surrounding pH on protein coating was analyzed for TiO_2 particles.

RESULTS

Both Human Lung Epithelial Cells and Human Monocyte-Derived Macrophages Take up Nanoparticles and Carbon Nanotubes. Transmission electron microscopy (TEM) was used to study intracellular localization of engineered materials. TEM pictures showed that all tested ENM-species ($n = 11$) were taken up by epithelial cells and primary macrophages after exposure to nanomaterials (5 or 300 μg/mL) for 24 h. Contrary to the 5 μg/mL experiments, most of the ENMs in higher concentration had agglomerated in the used cell culture media and only few individual particles were seen in TEM images. Materials behaved similarly in both cell types despite the differences in compositions of the growth media. The intracellular localization between particle−species differed, while no particles were detected in the nucleus. r/aTiO_2 (nanosized rutile/anatase titanium dioxide), rTiO_2 silica-coated (silica-coated nanosized rutile titanium dioxide), rTiO_2 alumina-coated (alumina-coated nanosized rutile titanium dioxide-), mwCNT (nanosized multiwalled carbon nanotube) and aTiO_2 (nanosized anatase titanium dioxide) nanomaterials were observed both inside vacuolar structures and free in the cytoplasm (Figure 1 and Supporting Information Figures 1−4) in both used exposure concentrations. The remainder of the materials were mainly found inside vacuolar structures. Only mwCNTs appeared to be able to enter cells passively through plasma membrane (Supporting Information Figure 2, arrowhead). Effective crossing of different biological barriers has been shown for CNTs also under endocytosis-inhibiting conditions and without an active energy-dependent uptake system.[18] Some nanoparticles were surrounded by membrane-structures resembling lysosomes by morphology (Figure 1 I, black arrow). Microscale particles were seen inside vacuoles (Supporting Information Figures 1−4), although the localization was difficult to determine because of the breakages induced to the thin sections due to the large size of the particles. Few individual ZnO (nanosized zinc oxide) particles were detected inside the cells (Supporting Information Figures 3 and 4, black arrows) after 5 μg/mL exposure. Localization of ZnO particles could not be defined in the higher exposure conditions, because both cell types appeared to be dead, which was most probably due to free zinc ions dissolved from the particles.

Nanomaterial−Protein Interactions Depend on the Surface Properties. Particle−protein interaction assay was performed to measure quantitative differences of the protein adsorption between various ENM-species and to determine whether there is a characteristic preference for binding of certain type of proteins either from blood plasma or cell lysate. All tested materials attached to plasma proteins, whereas adsorption toward cell lysate proteins diverged more both in the amount and specificity of binding (Figure 2A). Three forms of nanosized titanium dioxide showed highest affinity toward proteins. This was observed for human plasma as well as for primary macrophage and epithelial cell lysates. Hydrophobic rTiO_2 silicone-coated (silicone-coated nanosized rutile titanium dioxide) and swCNT (nanosized single-walled carbon nanotube) were not covered by cellular proteins at all, whereas few plasma proteins stuck to them. Microscale particles, rTiO_2 coarse (fine-sized rutile titanium dioxide) and quartz sand (MIN-U-SIL5) showed higher adsorption to plasma proteins than to proteins in cell lysate. The same effect could also be seen with alumina-coated rTiO_2, mwCNT, and SiO_2 (nanosized amorphous silica). Adsorption of proteins might have led to enhanced aggregation of ZnO particles causing the observed variability in the amounts of ZnO attached proteins between experiments as is seen in Figure 2 panels A and B.

Regardless of the used plasma protein concentrations rTiO_2 silica-coated, r/aTiO_2, aTiO_2, SiO_2, and quartz sand adsorbed the same amount of proteins. Whereas binding capacities of the other tested particles depended on the plasma protein concentration, showing 2−5 times higher adsorption with undiluted plasma. Total amount of adsorbed plasma proteins correlated slightly with the size of nanoparticles so that the larger the size is, the higher is the adsorption (Supporting Information 5). A similar connection between the primary or dispersion size of ENM and protein adsorption was not seen with cell lysate proteins, neither was there any obvious link between the bound protein quantity and zeta-potential, specific surface area, nor polyform of the nanomaterials. Adsorption of biomolecules may also lead to aggregation of ENMs[14,19] and thus change their active protein interaction surface area and the total amount of bound protein.
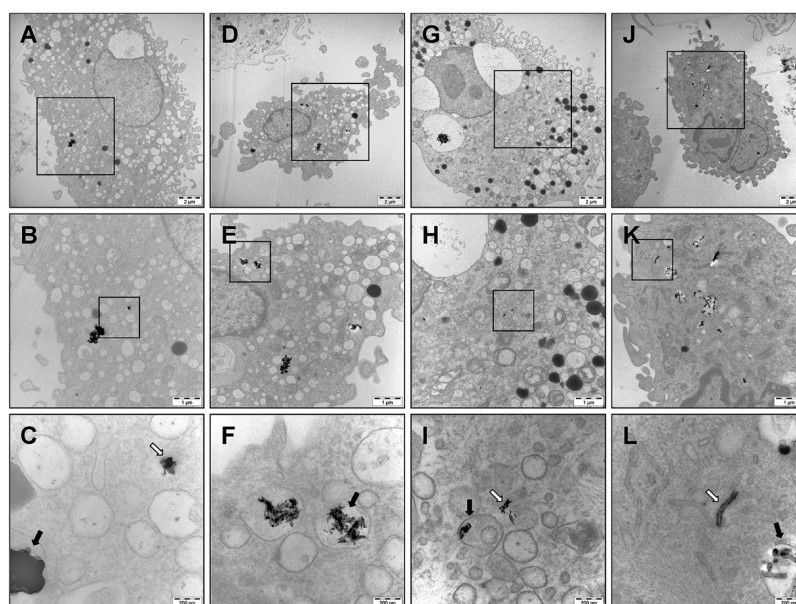
Figure 1. TEM images of human primary macrophages exposed to different ENMs (5 μg/mL) for 24 h. r/aTiO$_2$ exposed cells with 8000$\times$ magnification (A), caption with 20 000$\times$ magnification (B) and caption with 100 000$\times$ magnification (C). rTiO$_2$ silica$-$coated (D$-$F), rTiO$_2$ alumina-coated (G$-$I), mwCNT (J$-$L). Black and white arrows represent particles inside or outside vesicular structures, respectively.

The addition of surfactant to the epithelial cell lysate ENM binding assay showed that surfactant diminished the overall protein$-$ENM interaction substantially (Figure 2B). This reduction in the protein adsorption capacity was statistically significant for the ENMs that bind proteins best (Figure 2B bars 2$-$4) as the unpaired Student's t test p-values were below 0.05 for rTiO$_2$ silica-coated, r/aTiO$_2$ and aTiO$_2$. According to mass spectrometric protein identifications from the gel lanes, ENMs seemed to interact with the same proteins irrespective of whether surfactant was present or not, but the total amount of protein adsorption was lower. Pulmonary surfactant-associated protein B was among the major attached proteins on the surface of ENMs.

ENMs interacted also with few proteins from A549 cell culture medium (data not shown). However, the quantity of the protein adsorption from growth media was only a small fraction compared to protein binding from plasma or cell lysates.

The protein binding patterns of different ENMs in plasma and primary macrophage cell lysate after overnight incubation is illustrated in Figure 2C. Adsorption of plasma proteins to the surface of ENMs was also analyzed for 1 h interaction time, as there should be a change of bound proteins in the course of time.[20] However, with the used detergent containing buffer, equal amounts and the same major proteins were observed to be bound in both of the tested time points. These major plasma protein bands can be seen adsorbed to every particle (Figure 2C, lanes 1$-$6a). They were identified by mass spectrometry as fibrinogen alpha (I), beta (II) and gamma (III) chains and immunoglobulin light chain proteins (IV), all of which interact strongly with rTiO$_2$ silica-coated and aTiO$_2$. Other identified plasma proteins included several complement component proteins, fibronectin, apolipoprotein A, albumin, and fibrin. Adsorbed proteins were all glycosylated, which is a common modification for plasma proteins.

Primary macrophage cell lysate and epithelial cell lysate on the other hand, showed different binding patterns between particles. Lanes 1$-$6b in Figure 2C show that rTiO$_2$ silica-coated, r/aTiO$_2$, and aTiO$_2$ adhered to the same major cellular proteins but differences could be seen in less abundant proteins. rTiO$_2$ coarse particles had different affinity toward proteins compared to nanosized titanium dioxide primary macrophage cell lysates (Figure 2C, lane 5b). Although the protein binding profile was similar to the other TiO$_2$ particles in plasma, rTiO$_2$ alumina-coated did not interact significantly with proteins from cell lysates (Figure 2C, lane 1b).

Identification of ENM-Bound Cytoplasmic Proteins Reveals Selective Binding. To understand the effects of ENM$-$protein interactions on cell functions, nanoparticle-bound cytoplasmic proteins were identified by tandem mass spectrometry. Comparison between 79 most abundant proteins indentified from the untreated cytoplasm and proteins bound to different ENMs showed that the proteins adsorbed to the surfaces of rTiO$_2$ silica and aTiO$_2$ are identical with those of the untreated cytoplasm up to 36% and 42% (Figure 2D). The least overlap was observed for r/aTiO$_2$ bound proteins, for which only 13 identifications out of 74 were similar to proteins in cytoplasm.

Classification of the bound proteins according to their theoretical isoelectric point (pI) (Figure 3A:1$-$6)
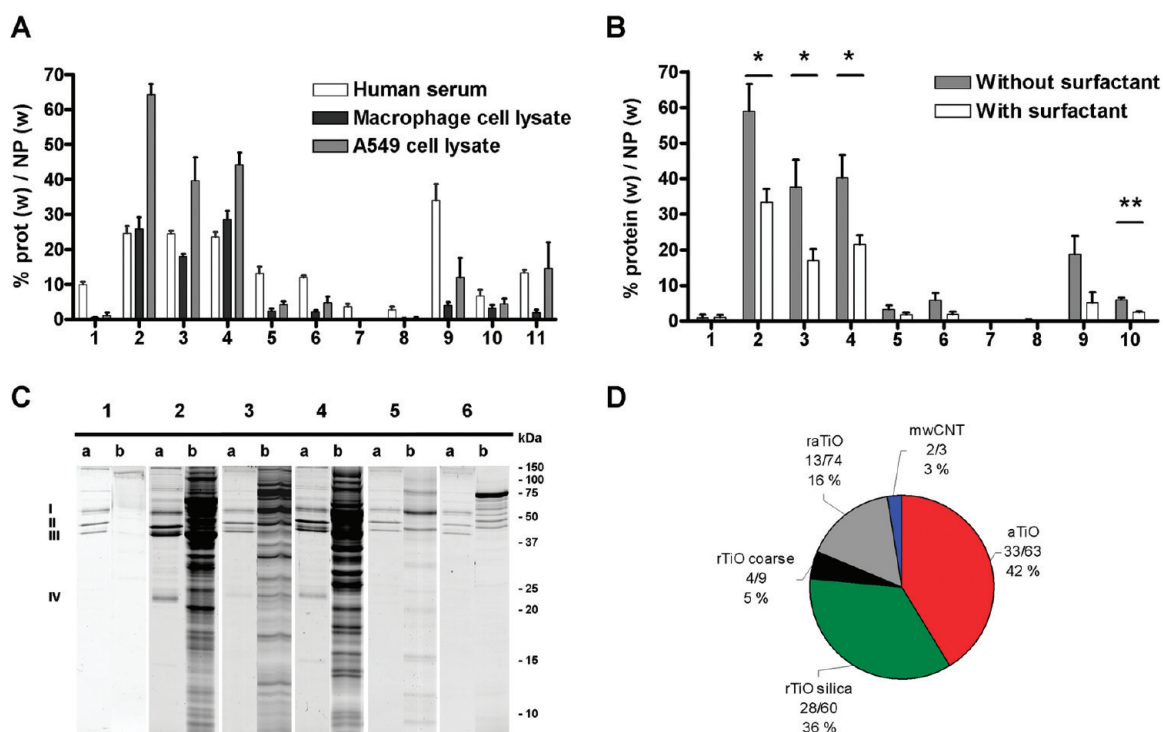
F3

C

Figure 2. Particle binding to blood plasma, primary macrophage cell lysate and A549 epithelial cell lysate proteins. (A) Protein-binding quantified as protein weight/particle weight percentage is shown for human blood plasma (white column), macrophage cell lysate (black column) and A549 epithelial cell lysate (gray column): rTiO₂ alumina-coated (1); rTiO₂ silica-coated (2); r/aTiO₂ (3); aTiO₂ (4); rTiO₂ coarse (5); mwCNT (6); swCNT (7); rTiO₂ silicone-coated (8); ZnO (9); MIN-U-SIL (10); SiO₂ (11). (B) Protein adsorption by ENMs from A549 epithelial cell lysate with (white columns) or without surfactant in the buffer (gray columns) represented as protein weight/particle weight percentage. Reduction of the binding capacity due to surfactant was statistically significant for rTiO₂ silica-coated, r/aTiO₂, and aTiO₂ (∗, $p > 0.0395, 0.0332,$ and 0.0264, respectively) and MIN-U-SIL (∗∗, $p > 0.0061$): rTiO₂ alumina-coated (1); rTiO₂ silica-coated (2); r/aTiO₂ (3); aTiO₂ (4); rTiO₂ coarse (5); mwCNT (6); swCNT (7); rTiO₂ silicone-coated (8); ZnO (9); MIN-U-SIL (10). (C) Coomassie-stained SDS-PAGE gel images illustrating protein binding patterns of different particles to human blood plasma (a) and primary macrophage cytoplasm (b): rTiO₂ alumina-coated (1); rTiO₂ silica-coated (2); r/aTiO₂ (3); aTiO₂ (4); rTiO₂ coarse (5); mwCNT (6); fibrinogen alpha chain I; fibrinogen beta chain II; fibrinogen gamma chain III; immunoglobulin kappa light chain IV. (D) Comparison of protein identifications of untreated cytoplasm with proteins adsorbed to different ENMs. Number of common identifications between ENM bound and cytoplasmic proteins/total number of identified proteins for each ENM; the percentage of common proteins in ENM to the 79 protein identifications in cytoplasm.

indicated that the surface charge of the TiO₂ particles partly defines the reactivity toward cytoplasmic proteins. As proteins carry a net positive charge at a pH below their isoelectric point, there is a tendency for higher pI containing proteins to interact with TiO₂ particles with a more negative zeta-potential, such as r/aTiO₂ and rTiO₂ coarse.

Gene ontology (GO) classification by function of extracted cytoplasmic proteins from primary macrophages is shown in Figure 3B:1–6. Most of the 79 proteins identified in the cytoplasm without ENMs had a role in cytoskeleton (30%), in protein biosynthesis (26%), or in metabolism/catabolism (22%); these classes contained over two-thirds of the identified proteins. The remainder of the proteins were classified to inflammatory response (5%), cell signaling (9%), cellular transportation (5%), oxidative stress (2%), and other (1%) (3B:1). rTiO₂ silica-coated nanoparticles showed elevated affinity toward cell signaling proteins. Bound proteins, 60 in total, included almost twice more cell signaling proteins (16%) than in untreated cytoplasm, whereas percentage

of functional group of protein biosynthesis (18%) was considerably lower compared to untreated cytoplasm (Figure 3B:2). The GO classification of the 78 identified proteins interacting with r/aTiO₂ showed reduced adherence to cytoskeletal proteins (19%), whereas the percentage of proteins classified in the group "Other" function was considerably large (13%) (Figure 3B:3). Functional classification of aTiO₂-bound cytoplasmic proteins revealed highly similar GO percentages compared to unexposed cytoplasm (Figure 3B:4). When interactions of rTiO₂ coarse particles to cytoplasmic proteins were analyzed, particularly proteins relating to protein biosynthesis (40%) and oxidative stress (10%) exhibited increased adherence (Figure 3B:5). Interestingly, mwCNTs seemed to bind only filamentous proteins of cytoskeleton; myosin, vimentin, and actin (Figure 3B:6).

All titanium dioxide particles analyzed above had affinity toward peroxiredoxin 1, annexin A2, and several ribosomal and cytoskeletal proteins. Proteins belonging to S100 calcium binding protein A family were

A

1

2

3

4

5

6

B

1

2
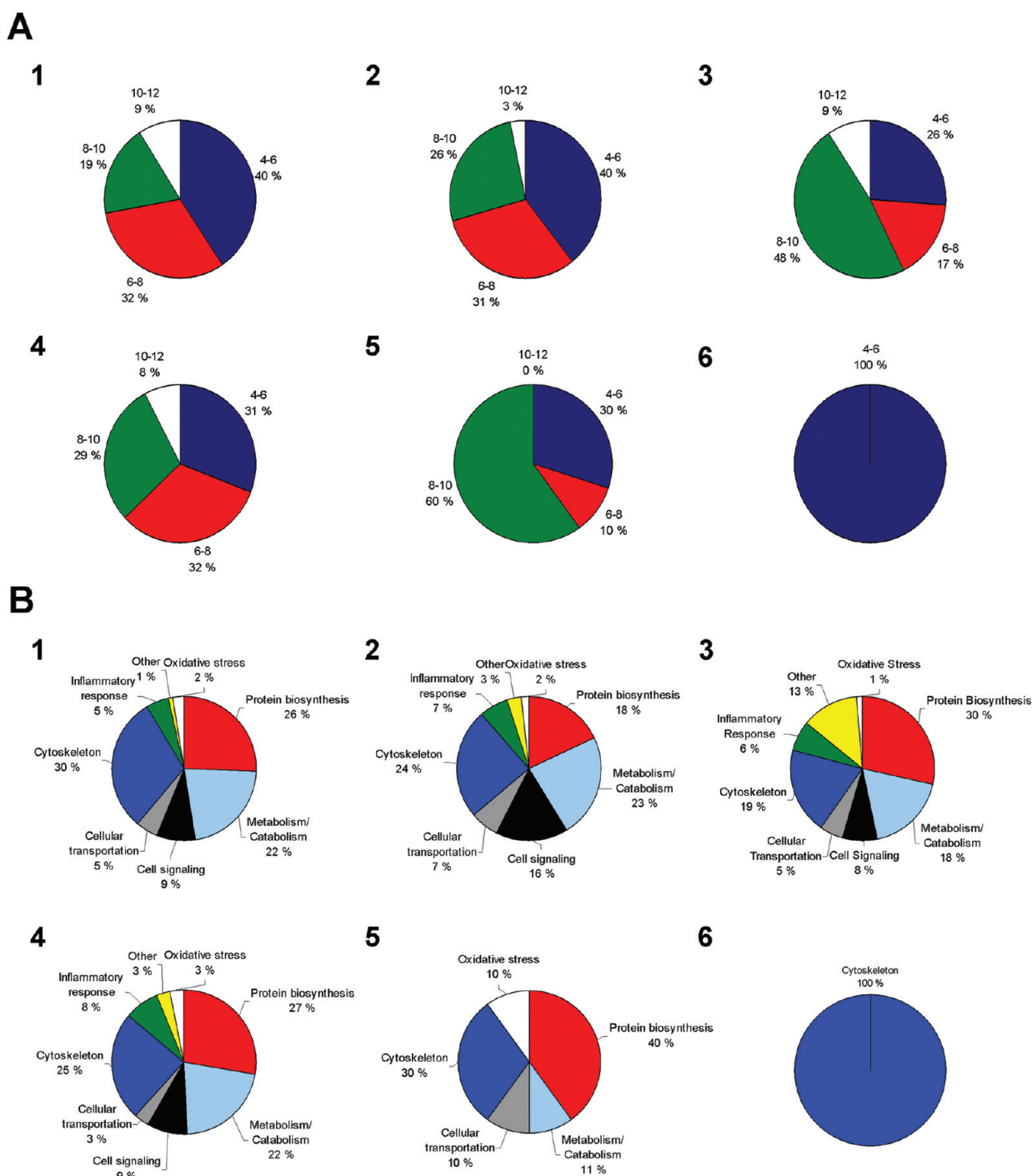

3

4

5

6

Figure 3. Classification of nanoparticle bound proteins from primary macrophage cytoplasm according to the calculated isoelectric points of the identified proteins (A:1—6) and according to function by gene ontology (B:1—6). Grouped cytoplasmic proteins are from incubations of cytoplasm without ENMs (1) or with rTiO$_2$ silica-coated (2), r/aTiO$_2$ (3), aTiO$_2$ (4), rTiO$_2$ coarse (5), and mwCNT (6), respectively.

identified only from nanoscaled TiO$_2$ particles. Calcium-binding domains of this protein family are rich in the negatively charged amino acids,[21] which might be involved in the interaction with these particles.

Depending on the pH Value of the Buffer Nanosized and Fine-Sized TiO$_2$ Particles Show Different Binding Affinities to Cell Lysate Proteins. Fine-sized TiO$_2$ material is used for selective enrichment of phosphorylated peptides.[12] Because some forms of the tested nanosized titanium dioxides bind cellular proteins more effectively than the coarse form, a protein adsorption experiment was carried out in three different pH values with primary macrophage cell lysate. The affinity of nanosized r/aTiO$_2$ particles to cell lysate proteins decreased only slightly when the pH of the solution increased, whereas protein binding capability of rTiO$_2$ coarse particles is totally lost at higher pH (Figure
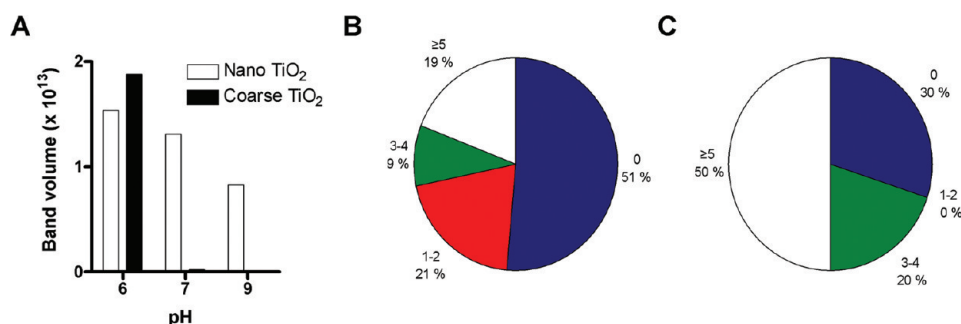
Figure 4. Comparison of binding of nanoscale and microscale TiO$_2$-particles to primary macrophage cell lysate proteins. Effect of pH on protein adsorptions to nanoscale r/aTiO$_2$ (white column) and to microscale rTiO$_2$ (black column) particles in different buffers were quantified from SDS-PAGE band volume in pH 6 (zeta-potential was -2 mV for both particles), in pH 7 (zeta-potentials were -62 and -73 mV), and in pH 9 (zeta-potentials were -37 and -46 mV) (A). Distribution of the bound proteins from nanoscale r/aTiO$_2$ (B) and microscale rTiO$_2$ (C) particles according to the number of phosphorylation sites in the identified proteins.

F4 4A). Also the selectivity for the number of phosphorylation sites in the identified proteins was different, because nanosized r/aTiO$_2$ particles adsorbed mostly nonphosphorylated proteins (Figure 4B) and rTiO$_2$ coarse particles showed preference for multiply phosphorylated compounds (Figure 4C). Results indicated clearly that nanoscale TiO$_2$ particles possessed different surface chemistry compared to the amphoteric ion-exchange properties displayed by rTiO$_2$ coarse particles and that the more efficient protein binding of nanosized TiO$_2$ particles was not due to larger surface area as such.

DISCUSSION

The obtained results shed light on the interactions between engineered nanomaterials and proteins at a cellular level in relation to surface chemistry. To understand the basis of the toxicity caused by ENMs, we scrutinize the first events that occur after the exposure: particle−protein interactions in the mucosa followed by entry to phagocytic and endothelial cells and finally interaction of ENMs with cellular proteins. We show that ENMs are able to enter cells and react with cellular proteins, thereby affecting cell operations by impairing normal protein functions.

Consistent with the findings reported here, many groups have demonstrated both *in vitro* and *in vivo* that ENMs are internalized by macrophages and lung epithelial cells.[5,22,23] Most of the particles seem to be located inside vesicular structures. This suggests that particles are taken up actively by phagocytosis, macropinocytosis, clathrin-mediated endocytosis, or by caveolae-mediated endocytosis as reviewed by Unfried *et al.*[24] The only particle species that might be able to enter cells passively by diffusion is mwCNT.[18] In contrast to our results, recent work by Tabet *et al.* suggested that epithelial cells are unable to internalize mwCNTs.[25] While there are indications that some ENMs might be able to enter nucleus,[24] none of the materials tested here were detected inside nucleus in TEM pictures.

ENM−protein interaction studies have mainly concentrated on ENM−plasma protein interactions, where nanoparticles are suggested to be coated by proteins to form a protein-corona.[7] The Vroman effect is used to describe the complex protein adsorption from blood onto particle surface.[20] The most abundant proteins arrive first and are later substituted by lower concentration proteins that have a higher affinity for the ENPs. According to the Vroman effect, albumin was displaced from ENMs when particles were first coated with bovine serum albumin before allowing them to interact with cell lysate proteins. Hellstrand *et al.*[26] have described a nanoparticle lipid corona after interaction studies with whole plasma. They showed that high-density lipoproteins such as apolipoproteins adhere strongly to copolymer nanoparticles. The present study shows that some of the nanosized TiO$_2$ particles are able to bind significantly more plasma and cell lysate proteins than other particles. The main plasma proteins that form the protein corona of ENMs are identified as fibrinogen alpha, beta, and gamma chains and immunoglobulin light chain. Fibrinogen is usually replaced from the interface by other plasma proteins, but in the used interaction conditions this did not occur, probably due to structural changes in the protein domains.[27] With the exception of nanosized rTiO$_2$ silica-coated, r/aTiO$_2$, and aTiO$_2$, other ENMs bind less cell lysate proteins than plasma proteins. This could originate from the different natures of plasma and cell lysate proteins; plasma proteins usually contain sugar moieties, which are less common among cytoplasmic proteins. In fact all identified plasma proteins adhering to ENMs are glycosylated. Because all the ENMs are coated by similar plasma proteins, opsonization could be the main reason behind the formation of a protein-corona in plasma. Foreign particles are opsonized by a set of proteins in the blood to facilitate their recognition and removal by cells of the reticuloendothelial system.[28] Although fibrinogen is the most active protein to adhere with the ENMs (Figure 2C, I, II and III), mass spectrometric analysis shows that complement proteins, fibronectin, immunoglobulins, and apolipoproteins are also attached.

Surfactant affects the interaction between ENMs and cell lysate proteins by reducing the amount of bound proteins (Figure 2B). Phospholipids, which are the major components of the pulmonary surfactant, could be competing with cell lysate phosphoproteins for adsorption on the surface of ENMs. Results suggest, however, that the effect is quantitative rather than qualitative.

Because of the diverse population of engineered nanomaterials and large variation in their surface coatings it is important to discriminate if the toxicological effects observed are caused by the material itself, surface coating, an impurity, or some material used in the synthesis of it. Solubility and optical characteristics of the particles are easily modified by surface coating, which also changes their surface chemistry. Larger surface area improves the ability of particles to interact with the surroundings, but it seems that the surface chemistry is even more critical in the case of protein adsorption. The effect of particle coating can be seen in the binding of cell lysate proteins to different TiO_2-species: uncoated anatase and rutile phases of TiO_2 adsorb proteins similarly, whereas alumina and silicone-coated rutile forms of TiO_2 bind only a few proteins.

When comparing protein adsorption between swCNT and $rTiO_2$ silica-coated, even though having larger surface area, swCNT binds less proteins. Solubility, which depends on particle zeta potential in solution, is one of the determinants of surface reactivity of a given particle.[11] Here, particle solubility does not seem to cause the variation in the efficiency of protein adsorption by ENMs, and neither does the specific surface area nor the polyform of nanosized particles. It is evident that truly hydrophobic particles such as $rTiO_2$ silicone-coated are not able to bind proteins. It is not known, however, which physicochemical properties induce the clear distinction in protein adherence of the two ENPs, $rTiO_2$ silica-coated and $rTiO_2$ alumina-coated, which share common size, zeta potential, surface area, and even phase structure.

Chromosomal instability caused by fibers binding to proteins regulating cytoskeleton organization and mitotic processes during mitosis has already been shown with asbestos fibers by MacCorkle et al.[29] Similarly, another fibrous material, mwCNT, interacts solely with cytoskeletal proteins, mainly vimentin. The cytoskeleton has also been shown to be actively involved in the uptake of quartz particles by alveolar macrophages.[30] Identified adsorbed cytoplasmic proteins play roles in metabolism, protein biosynthesis, response to stress, and cell differentiation; thus the toxicological effects of nanomaterials could be mediated by interactions with cytoplasmic proteins. Owing to variability in the types of proteins adsorbed on ENMs, the toxicological effects of ENM-species could arise from different mechanisms.

Fine-sized titanium dioxide is used for the extraction of phosphorylated proteins from complex protein mixtures.[31] It interacts with proteins very effectively at pH 6 by mechanisms that are not fully understood, while the binding ability quickly disappears in more basic pH values. For nanosized TiO_2 the binding is different, as the detachment of proteins is less dramatic than for fine-sized TiO_2. Results suggest that pH alters the surface reactivity of particles and thus affects noncovalent interactions between particles and proteins. The effect of pH on protein adsorption exemplifies a novel mechanism to toxic action of ENMs: after particles are phagocytosized by cells, particles are inside phagosomes which mature gradually to lysosomes in which the pH is markedly lower than in the cytoplasm.[24] The low pH would enhance adsorption of nanoscaled TiO_2 particles to the lysosomal proteins, therefore contributing to the possible release of particles into the cytoplasm subsequent to lysosomal rupture.

Our study demonstrates that cells of the respiratory tract actively phagocytosize opsonized ENMs and capture them inside vesicular structures. Some species of nanoparticles might then be able to escape vesicular structures, with the possible role played by acidic lysosomal pH, and end up in the cytoplasm. This exposes cytoplasmic proteins to ENMs, thus allowing ENM−protein interactions, which in turn might inflict cellular damage. As proteins are usually the first species to arrive at a freshly formed particle interface, understanding the mechanism and the relevance of particle uptake could aid in the determination of toxic effects of particles as well as in the search for biocompatible materials. We propose the particle−protein binding assay to be included in routine analysis of particle properties as it offers novel information about the surface reactivity and therefore can help assess the safety of ENMs.

METHODS

Materials Used. Eleven different types of commercial particles were used in the experiments. Five forms of titanium dioxide (TiO_2) nanoparticles and one coarse TiO_2 material were studied: fine-sized rutile ($rTiO_2$ coarse; Sigma-Aldrich, Steinheim, Germany), nanosized rutile/anatase ($r/aTiO_2$; NanoAmor, Nanostructured and Amorphous Materials Inc., Houston, TX), nanosized anatase ($aTiO_2$; Sigma-Aldrich, Steinheim, Germany), silica-coated nanosized rutile ($rTiO_2$ silica-coated; Sigma-Aldrich, Steinheim, Germany), alumina-coated rutile ($rTiO_2$ alumina-coated; Kemira, Helsinki, Finland), silicone-coated rutile ($rTiO_2$ silicone-coated; Kemira, Helsinki, Finland). Other analyzed nanosized metal oxide particles were

TABLE 1. Characteristics of Materials Used in the Experiment

name	vendor	pr. number	particle size: primary (in dispersion)	specific surface area	zeta-potential	phase	composition
rTiO$_2$ silica-coated	Sigma-Aldrich	637262	10 × 40 nm (3.4 μm)	132 m^2/g (130—190 m^2/g by S-A)	−38 mV	rutile	Ti, O, SiO$_2$ coating (<5% by S-A)
rTiO$_2$ alumina-coated	Kemira	UV-TITAN M111	~14 nm (0.1 and 0.6 μm)	112 m^2/g (~100 m^2/g by Kemira)	−47 mV	rutile	Ti, O, alumina coating (~3% by Kemira)
rTiO$_2$ silicone-coated	Kemira	UV-TITAN M170	~14 nm (1 and 5.3 μm)	84 m^2/g (~80 m^2/g by Kemira)	−10 mV	rutile	Ti, O, alumina coating + silicone treatment
r/aTiO$_2$	NanoAmor	5485HT	30—40 nm (3.2 μm)	23 m^2/g (~30 m^2/g by NA)	−62 mV	rutile + anatase	Ti, 0
aTiO$_2$	Sigma-Aldrich	637254	<25 nm (1.3 μm)	222 m^2/g (210—220 m^2/g by S-A)	−40 mV	anatase	Ti, 0
rTiO$_2$ coarse	Sigma-Aldrich	224227	<5 μm (1.3 μm)	2 m^2/g	−73 mV	rutile	Ti, 0
ZnO	Umicore	ZANO	30—35 nm (0.2 and >6 μm)	22 m^2/g	−27 mV	zincite	Zn, 0
SiO$_2$	NanoAmor	4850MR	10 nm (0.65 and 4.9 μm)	515 m^2/g (~640 m^2/g by NA)	−43 mV	amorphous	Si, 0
mwCNT	SES Research	900-1260	10—30 nm x 1—2 μm (0.5 and 4.9 μm)	60 m^2/g	−50 mV	CNT	C, Ni (0.2%, catalyst residual)
swCNT	SES Research	900-1351	<2 nm x 1—5 μm (0.1 - 2.5 μm)	436 m^2/g	−43 mV	CNT	C, Co (0.6%, catalyst residual)
quartz sand	US Silica	MIN-U-SIL5	<5 μm (1.3 μm)	4 m^2/g	−70 mV	quartz	Si, 0

zinc oxide (ZnO; Umicore, Brussels, Belgium) and amorphous silica (SiO$_2$; NanoAmor, Nanostructured and Amorphous Materials Inc., Houston, TX). As properties of the latter material were changing during the time in storage (Supporting Information 6), SiO$_2$ results were excluded from the studies with surfactant. Two types of carbon nanotubes were tested, single-walled and multiwalled (swCNT and mwCNT, respectively; SES Research GMBH, Hamburg, Germany). Fine-sized quartz sand (MIN-U-SIL5; US Silica Company, Berkeley Springs, VW) was used as a positive toxicological control. All materials were characterized before exposures (specific characteristics are shown in Table 1). The composition of the particles was determined by energy dispersive spectroscopy (EDS; Thermo-Noran Vantage, Thermo Scientific, Breda, The Netherlands) attached in transmission electron microscope. The crystallinity and phase structure of nanopowders were characterized with X-ray diffractometer (Siemens D-500, Siemens AG, Karlsruhe, Germany), and specific surface area of the used nanomaterials was measured by adsorption, using the Brunauer—Emmett—Teller (BET) method (Coulter Omnisorp 100CX, Florida). Morphology of the materials was determined with scanning electron microscope SEM (Zeiss ULTRAplus FEG-SEM, Carl Zeiss NTS GmbH, Oberkochen, Germany). SEM images of ENMs are shown in Supporting Information Figure 7.

Surface Charge and Particle Size Analyses in Dispersion. Zeta potentials (surface charges) and particle sizes of the ME lysis buffer (1% Nonidet P40, 0.5% sodium deoxycholate, 80 mM MOPS, 2 mM EDTA pH 7.2) dispersed ENMs (0.5 mg/mL) were sonicated mildly for 15 min in an ultrasonic bath (USF Finnsonic W-181-T, Ultra Sonic Finland, Finland) before measurements with Zetasizer Nano ZS instrument (Malvern Instruments Inc., UK). The principle of the measurement is described by Jiang et al.[32] Size distribution in dispersion was hard to measure for some of the materials: ZnO dispersion contain over 6 μm agglomerates and swCNT showed polydisperse size distribution. The mean particle sizes of rTiO$_2$ silica, aTiO$_2$, mwCNT, and swCNT in dispersions having various additives such as albumin, serum, or phospholipids are shown in Vippola et al.[33] Materials themselves did not have a significant effect on the pH of buffer.

Cell Culture. Human lung epithelial cell line A549 (ATCC, Manassas, VA, US) and human monocyte-derived macrophages from buffy coats (The Finnish Red Cross Blood Transfusion Service, Helsinki, Finland) were used to study the intracellular localization of nanoparticles by electron microscopy and to acquire information on binding of nanoparticles to cellular proteins.

Epithelial cells were cultured in RPMI 1640 medium (Invitrogen, Carlsbad, CA) supplemented with 10% of heat inactivated fetal bovine serum (FBS), 1% penicillin—streptomycin (PEST) antibiotics and 2 mM L-glutamine. All cells were grown in +37 °C 5% CO$_2$. The differentiation of macrophages was performed by isolating peripheral blood mononuclear cells from the buffy coats by Ficoll—Paque-gradient centrifugation after which the mononuclear cell layer was harvested. After the harvested cells were washed three times with phosphate buffered saline (PBS) (pH 7.4), the mononuclear cells were allowed to adhere onto six-well plates (1.4 million cells/well) 50 min in RPMI 1640 medium supplemented with 2 mM L-glutamine and 1% PEST in +37 °C 5% CO$_2$. The cells were then washed three times with PBS and after the last wash the adhered cells were given 0.5 mL Serum-Free Macrophage medium (Invitrogen, Carlsbad, CA, US) supplemented with 10 ng/mL granulocyte-macrophage colony-stimulating factor (GM-CSF, ImmunoTools, GmbH, Germany) and 1% PEST. The macrophage medium was changed every 2 days. Maturated macrophages were used for exposure studies on the seventh day after the cell harvesting.

***In Vitro* Exposure Conditions for TEM Analysis.** Prior to all *in vitro* exposures, nanomaterials were sonicated for 15 min in an ultrasonic bath. Bovine serum albumin (BSA) concentrations were on the same level (10 and 5 mg/mL) in the both cell culture media (see below). Primary macrophages were exposed to 5 or 300 μg/mL of nanomaterials in Serum-Free Macrophage medium supplemented with 10 ng/mL GM-CSF, 1% PEST, and 1% BSA (Sigma-Aldrich, St. Louis, MO) and incubated 24 h in +37 °C 5% CO$_2$. BSA was added to reduce agglomeration of the nanomaterials. The next day, cells were washed two times with

PBS (pH 7.4), fixed with 2.5% glutaraldehyde in 0.1 M phosphate buffer, and removed from the plate by scraping.

Exposure to epithelial cells was carried out with 5 or 300 μg/mL of sonicated (15 min) ENMs in RPMI 16400 medium containing 10% of heat inactivated (FBS), 1% PEST antibiotics, and 2 mM L-glutamine. Cells were exposed for 24 h in +37 °C 5% CO_2, washed two times with PBS, removed from the plate by trypsination, and fixed with 2.5% glutaraldehyde in 0.1 M phosphate buffer.

Electron Microscopy. After fixation, cells were postfixed in 1% osmium tetroxide, dehydrated and embedded in Epon. Thin sections were collected on uncoated copper grids, stained with uranyl acetate and lead citrate, and then examined with a transmission electron microscope operated at an acceleration voltage of 80 KV (JEM-1220, Jeol Ltd., Tokyo, Japan).

Protein−Nanomaterial Interaction Experiments. The method for analysis of protein−ENM interaction was modified from Mac-Corkle in vitro.[29] Cells (primary macrophages or epithelial cells) were collected, frozen, and lysed with ME lysis buffer containing protease inhibitor (Complete Mini, Roche Diagnostics GMBH, Mannheim, Germany) for 20 min on ice. Cell lysate (~1 mg protein/mL) was cleared by centrifugation (16000g, 5 min, +4 °C) and exposed to sonicated (15 min) ENMs in ME lysis buffer. Final nanomaterial concentrations of 0.5, 0.05, or 0.005 mg/mL were used for the interaction experiments. While the lowest ENM concentration could not be analyzed due to the detection limit of gel stain, the results from the 0.05 mg/mL assay can be seen in Supporting Information Figure 6. Experiments with 50 μg/mL ENM concentration show that the binding pattern is similar to that of the 0.5 mg/mL concentration assays, but as the amount of binding is significantly lower, the ENM concentration of 0.5 mg/mL was chosen for studies. Alternatively, diluted human plasma in the ME buffer (~7 mg protein/ml), undiluted plasma (70 mg protein/mL), or A549 cell culture medium (~7 mg protein/ml) was used. To avoid unspecific adsorption of proteins to the walls of the test-tubes, low protein binding tubes were used (Protein LoBind tube, Eppendorf AG, Hamburg, Germany). The nanomaterial-cell lysate/plasma mixture was incubated at +4 °C for 15 h (or also 1 h for plasma) in an end-to-end rotator (Grant-Bio PTR-30, Wolf Laboratories Limited, UK), after which nanomaterials were pelleted and unbound proteins were removed by washing the pellet six times with 20 mM Tris-MOPS, pH 7.4. After each wash nanomaterials were gently vortexed and centrifuged (16000g, 5 min, +4 °C). The washes were saved and analyzed in SDS-polyacrylamide gel electrophoresis (SDS-PAGE) to ensure that the amount of washes was sufficient to remove all unbound proteins. ENM-bound proteins were removed from the nanomaterials by heating for 10 min at +70 °C in 50 μL reducing sample buffer (62.5 mM Tris-HCl pH 6.8, 5% β-mercaptoethanol, 2% bromophenol blue, 2% SDS, 25% glycerol) and analyzed in SDS-PAGE. Because some proteins may stay attached to ENMs, for example as described in Schulze et al.,[34] ENM containing gel-pockets (stacking gel was not removed) were also stained for residual protein binding after SDS-PAGE; however, no protein staining was observed suggesting that practically all adsorbed proteins were detached from the ENM during the treatment. Gels were stained with Coomassie blue dye (0.1% Serva Blau G, 50% methanol, 1% acetic acid) and excess dye was removed from gels with destaining solution (20% methanol, 1% acetic acid). Gels were scanned, and the intensities of Coomassie stained protein bands were calculated with ImageQuant TL (GE Healthcare, Piscataway, NJ) software to quantify protein binding to nanomaterials. Protein band intensities were compared to the intensity of a protein band with the known amount of protein analyzed in the same SDS-PAGE gel. Statistical analyses were performed using GraphPad Prism 4 software (GraphPad Software, La Jolla, CA). Protein concentrations were determined with Bio-Rad DC Protein Assay (Bio Rad, Hercules, CA).

The effect of surfactant on protein−ENM interactions was studied by incubating natural porcine lung surfactant mixture (Curosurf, Nycomed International Management GmbH, Zurich, Switzerland) with sonicated nanomaterials in ME buffer (final concentration 1.2 μg/mL). After 15 min A549 epithelial cell lysate was added to the mixture. Incubation and analysis were performed as described above.

For protein−ENM interaction studies with cytoplasmic proteins, cytoplasm was extracted from primary macrophage cells with ProteoJet Cytoplasmic and Nuclear Protein Extraction Kit (Fermentas International Inc., Burlington, ON, Canada) and mixed with sonicated nanoparticles in ME lysis buffer (final nanoparticle concentration, 0.5 mg/mL) for 15 h at +4 °C in an end-to-end rotator. The removal of unbound proteins and analysis of bound proteins were carried out as described above.

The effect of pH on nanomaterial binding to proteins was studied with rTiO$_2$ coarse and r/aTiO$_2$ particles. A 200 μL portion of cleared primary macrophage-cell lysate was exposed to 100 μL of sonicated particles (5 mg/mL) in ME lysis buffer and to 700 μL of different pH buffers. The binding of particles to proteins was analyzed as previously described. Buffers were pH 6 (250 mM sodium acetate), pH 7.2 (ME lysis buffer), and pH 9 (100 mM Tris-HCl).

Identification of Nanomaterial-Bound Proteins. Coomassie-stained protein bands were cut from the gel and in-gel digested, and the resulting peptides were extracted as previously described by Korolainen et al.[35] Peptide extracts were pooled and dried in a vacuum centrifuge. Each peptide mixture was analyzed by automated nanoflow capillary liquid chromatography−tandem mass spectrometry (LC−MS/MS) using a CapLC system (Waters, Milford, MA) coupled to an electrospray ionization quadrupole time-of-flight mass spectrometer (Q-TOF Global, Waters). Reverse-phase separation of peptides was carried out using a 75 μm × 15 cm NanoEase Atlantis dC$_{18}$ column (Waters) at a flow rate of 250 nL/min. Peptides were eluted from the column with a linear gradient of 0−60% solvent B (0.1% formic acid in 95% acetonitrile) in 60 min. Solvent A was 0.1% formic acid in 5% acetonitrile. The obtained mass fragment spectra were searched in NCBInr database against human entries using in-house Mascot v.2.1 (Matrix Science Ltd., London, UK) (Supporting Information). Isoelectric point (pI) values were calculated from the nominal masses of protein hits in Mascot search. Information on phosphorylation modification and gene ontology were gathered from the protein knowledge-base of UniProt (www.uniprot.org).

Conflict of Interest: None.

Supporting Information Available: TEM-pictures of ENMs inside human epithelial cells and primary human macrophages; influence of different ENM concentrations on total adsorption of proteins, correlations between the amount of adsorbed protein and the physicochemical properties of tested materials, and morphology of studied materials by scanning electron microscopy; lists of identified proteins together with proteomic data. This material is available free of charge *via* the Internet at http://pubs.acs.org.

REFERENCES AND NOTES

1. Alexiou, C.; Jurgons, R.; Seliger, C.; Iro, H. Medical Applications of Magnetic Nanoparticles. *J. Nanosci. Nanotechnol.* **2006**, *6*, 2762–2768.

2. Avouris, P.; Chen, Z.; Perebeinos, V. Carbon-Based Electronics. *Nat. Nanotechnol.* **2007**, *2*, 605–615.

3. Lee, Y. J.; Ruby, D. S.; Peters, D. W.; McKenzie, B. B.; Hsu, J. W. ZnO Nanostructures as Efficient Antireflection Layers in Solar Cells. *Nano Lett.* **2008**, *8*, 1501–1505.

4. Lindberg, H. K.; Falck, G. C. -M.; Suhonen, S.; Vippola, M.; Vanhala, E.; Catalán, J.; Savolainen, K.; Norppa, H. Genotoxicity of Nanomaterials: DNA Damage and Micronuclei Induced by Carbon Nanotubes and Graphite Nanofibres in Human Bronchial Epithelial Cells *in Vitro*. *Toxicol. Lett.* **2009**, *186*, 166–173.

5. Rossi, E. M.; Pylkkänen, L.; Koivisto, A. J.; Vippola, M.; Jensen, K. A.; Miettinen, M.; Sirola, K.; Nykäsenoja, H.; Karisola, P.; Stjernvall, T.; *et al.* Airway Exposure to Silica-Coated TiO$_2$

Nanoparticles Induces Pulmonary Neutrophilia in Mice. *Toxicol. Sci.* **2010**, *113*, 422–433.

6. Takagi, A.; Hirose, A.; Nishimura, T.; Fukumori, N.; Ogata, A.; Ohashi, N.; Kitajima, S.; Kanno, J. Induction of Mesothelioma in p53± Mouse by Intraperitoneal Application of Multiwall Carbon Nanotube. *J. Toxicol. Sci.* **2008**, *33*, 105–116.

7. Cedervall, T.; Lynch, I.; Lindman, S.; Berggård, T.; Thulin, E.; Nilsson, H.; Dawson, K. A.; Linse, S. Understanding the Nanoparticle–Protein Corona Using Methods to Quantify Exchange Rates and Affinities of Proteins for Nanoparticles. *Proc. Natl. Acad. Sci. U.S.A.* **2007**, *104*, 2050–2055.

8. Chithrani, B. D.; Ghazani, A. A.; Chan, W. C. Determining the Size and Shape Dependence of Gold Nanoparticle Uptake into Mammalian Cells. *Nano Lett.* **2006**, *6*, 662–668.

9. McNeil, S. E. Nanotechnology for the Biologist. *J. Leukocyte Biol.* **2005**, *78*, 585–594.

10. Moghimi, S. M.; Davis, S. S. Innovations in Avoiding Particle Clearance from Blood by Kupffer Cells: Cause for Reflection. *Crit. Rev. Ther. Drug Carrier Syst.* **1994**, *11*, 31–59.

11. Fubini, B. Surface Reactivity in the Pathogenic Response to Particulates. *Environ. Health Perspect.* **1997**, *105*), 1013–1020.

12. Schmidt, S. R.; Schweikart, F.; Andersson, M. E. Current Methods for Phosphoprotein Isolation and Enrichment. *J. Chromatogr. B* **2007**, *849*, 154–162.

13. Oberdorster, G.; Oberdorster, E.; Oberdorster, J. Nanotoxicology: An Emerging Discipline Evolving from Studies of Ultrafine Particles. *Environ. Health Perspect.* **2005**, *113*, 823–839.

14. Bakshi, M. S.; Zhao, L.; Smith, R.; Possmayer, F.; Petersen, N. O. Metal Nanoparticle Pollutants Interfere with Pulmonary Surfactant Function *In Vitro. Biophys. J.* **2008**, *94*, 855–868.

15. Schleh, C.; Mühlfeld, C.; Pulskamp, K.; Schmiedl, A.; Nassimi, M.; Lauenstein, H. D.; Braun, A.; Krug, N.; Erpenbeck, V. J.; Hohlfeld, J. M. The Effect of Titanium Dioxide Nanoparticles on Pulmonary Surfactant Function and Ultrastructure. *Respir. Res.* **2009**, *10*, 90.

16. Herzog, E. L.; Brody, A. R.; Colby, T. V.; Mason, R.; Williams, M. C. Knowns and Unknowns of the Alveolus. *Proc. Am. Thorac. Soc.* **2008**, *5*, 778–782.

17. Hoet, P.; Bruske-Hohlfeld, I.; Salata, O. Nanoparticles—Known and Unknown Health Risks. *J. Nanobiotechnol.* **2004**, *2*, 12.

18. Kostarelos, K.; Lacerda, L.; Pastorin, G.; Wu, W.; Wieckowski, S.; Luangsivilay, J.; Godefroy, S.; Pantarotto, D.; Briand, J. P.; Muller, S.; *et al.* Cellular Uptake of Functionalized Carbon Nanotubes Is Independent of Functional Group and Cell Type. *Nat. Nanotechnol.* **2007**, *2*, 108–113.

19. Schleh, C.; Hohlfeld, J. M. Interaction of Nanoparticles with the Pulmonary Surfactant System. *Inhalation Toxicology* **2009**, *21*, 97–103.

20. Vroman, L.; Adams, A.; Fischer, G.; Munoz, P. Interaction of High Molecular Weight Kininogen, Factor XII, and Fibrinogen in Plasma at Interfaces. *Blood* **1980**, *55*, 156–159.

21. Santamaria-Kisiel, L.; Rintala-Dempsey, A. C.; Shaw, G. S. Calcium-Dependent and Independent Interactions of the S100 Protein Family. *Biochem. J.* **2006**, *396*, 201–214.

22. Simon-Deckers, A.; Gouget, B.; Mayne-L'Hermite, M.; Herlin-Boime, N.; Reynaud, C.; Carrière, M. *In Vitro* Investigation of Oxide Nanoparticle and Carbon Nanotube Toxicity and Intracellular Accumulation in A549 Human Pneumocytes. *Toxicology* **2008**, *253*, 137–146.

23. Stearns, R. C.; Paulauskis, J. D.; Godleski, J. J. Endocytosis of Ultrafine Particles by A549 Cells. *Am. J. Respir. Cell Mol. Biol.* **2001**, *24*, 108–115.

24. Unfried, K.; Albrecht, C.; Klotz, L.; Von Mikecz, A.; Grether-Beck, S.; Schins, R. P. F. Cellular Responses to Nanoparticles: Target Structures and Mechanisms. *Nanotoxicology* **2007**, *1*, 52–71.

25. Tabet, L.; Bussy, C.; Amara, N.; Setyan, A.; Grodet, A.; Rossi, M. J.; Pairon, J.; Boczkowski, J.; Lanone, S. Adverse Effects of Industrial Multiwalled Carbon Nanotubes on Human Pulmonary Cells. *J. Toxicol. Environ. Health, A: Curr. Iss.* **2009**, *72*, 60.

26. Hellstrand, E.; Lynch, I.; Andersson, A.; Drakenberg, T.; Dahlbäck, B.; Dawson, K. A.; Linse, S.; Cedervall, T. Complete High-Density Lipoproteins in Nanoparticle Corona. *FEBS J.* **2009**, *276*, 3372–3381.

27. Jung, S. Y.; Lim, S. M.; Albertorio, F.; Kim, G.; Gurau, M. C.; Yang, R. D.; Holden, M. A.; Cremer, P. S. The Vroman Effect: A Molecular Level Description of Fibrinogen Displacement. *J. Am. Chem. Soc.* **2003**, *125*, 12782–12786.

28. Owens, D. E., III; Peppas, N. A. Opsonization, Biodistribution, and Pharmacokinetics of Polymeric Nanoparticles. *Int. J. Pharm.* **2006**, *307*, 93–102.

29. MacCorkle, R. A.; Slattery, S. D.; Nash, D. R.; Brinkley, B. R. Intracellular Protein Binding to Asbestos Induces Aneuploidy in Human Lung Fibroblasts. *Cell Motil. Cytoskeleton* **2006**, *63*, 646–657.

30. Haberzettl, P.; Duffin, R.; Kramer, U.; Hohr, D.; Schins, R. P.; Borm, P. J.; Albrecht, C. Actin Plays a Crucial Role in the Phagocytosis and Biological Response to Respirable Quartz Particles in Macrophages. *Arch. Toxicol.* **2007**, *81*, 459–470.

31. Yu, Y. Q.; Fournier, J.; Gilar, M.; Gebler, J. C. Phosphopeptide Enrichment Using Microscale Titanium Dioxide Solid Phase Extraction. *J. Sep. Sci.* **2009**, *32*, 1189–1199.

32. Jiang, J.; Oberdörster, G.; Biswas, P. Characterization of Size, Surface Charge, and Agglomeration State of Nanoparticle Dispersions for Toxicological Studies. *J. Nanopart. Res.* **2009**, *11*, 77–89.

33. Vippola, M.; Falck, G. C. M.; Lindberg, H. H.; Suhonen, S.; Vanhala, E.; Norppa, H.; Savolainen, K.; Tossavainen, A.; Tuomi, T. Preparation of Nanoparticle Dispersions for *In Vitro* Toxicity Testing. *Hum. Exp. Toxicol.* **2009**, *28*, 377–385.

34. Shulze, C.; Schaefer, U. F.; Ruge, C. A.; Wohlleben, W.; Lehr, C. M. Interaction of Metal Oxide Nanoparticles with Lung Surfactant Protein A. *Eur. J. Pharm. Biopharm.* **2011**, *77*, 376–383.

35. Korolainen, M. A.; Goldsteins, G.; Nyman, T. A.; Alafuzoff, I.; Koistinaho, J.; Pirttilä, T. Oxidative Modification of Proteins in the Frontal Cortex of Alzheimer's Disease Brain. *Neurobiol. Aging* **2006**, *27*, 42–53.